

Dynamic analysis of piezoelectric perforated cantilever bimorph energy harvester via finite element analysis

Yousef A. Alessi¹, Ibrahim Ali¹, Mashhour A. Alazwari¹, Khalid Almitani¹,
Alaa A Abdelrahman² and Mohamed A. Eltaher*^{1,2}

¹Mechanical Engineering Department, Faculty of Engineering, King Abdulaziz University,
P.O. Box 80204, Jeddah 21589, Saudi Arabia

²Mechanical Design & Production Department, Faculty of Engineering, Zagazig University,
P.O. Box 44519, Zagazig 44519, Egypt

(Received April 3, 2023, Revised April 19, 2023, Accepted April 27, 2023)

Abstract. This article presents a numerical analysis to investigate the natural frequencies and harmonic response of a perforated cantilever beam attached to two layers of piezoelectric materials by using the finite element method for the first time. The bimorph piezoelectric is composed of 3 layers; two of them at the outer are piezoelectric, and the inner isotropic material. A higher order 3-D 20-node solid element that exhibits quadratic displacement behavior is exploited to discretize the isotropic layer, and coupled piezoelectric 3D element with twenty nodes is used to mesh the top and bottom layers. CIRC94 element is added to act as a resistor part of the model. The proposed model is validated with previous works. The numerical parametric studies are presented to illustrate the effects of perforation geometry, the number of rows, the resistance on the natural frequencies, frequency response, and power. It is found that the thickness has a positive relationship with the natural frequency. Perforations help in producing higher voltage, and the best shape is rectangular perforations, and to produce higher voltage, two rows of rectangular perforations should be applied.

Keywords: energy harvester; finite element analysis; perforated structures; piezoelectric bimorph

1. Introduction

Piezoelectricity is the phenomenon of developing electrical energy in the form of electric potential (voltage) on the surface of some materials that are under mechanical loads such as stress, pressure, or deformations. These materials also have the inverse effect of changing electric energy to mechanical energy as deformation or internal stresses. These materials are called piezoelectric materials, and they include different materials, either artificial or naturally found, Shabara *et al.* (2020). The discovery of ferroelectric materials is the main reason for having an enormous amount of manmade piezoelectric materials, as ferroelectric materials can possess piezoelectric behavior after performing a certain process. The process unites the direction of polarization of the ferroelectric material by applying direct electric current while the material is under high temperature for a period of time; then, the material is disconnected from the current and cold down

*Corresponding author, Professor, E-mail: mohaeltaher@gmail.com, meltaher@kau.edu.sa

to room temperature resulting in a permanent polarization of the material, Shabara *et al.* (2020). Since the discovery of piezoelectricity, it has been utilized in many applications as actuators or motors, performing the motion, sensors, generating electrical pulses, transformers, and lastly, benders, Badr and Ali (2011), Najafi (2022). Using Kirchhoff's thin plate theory, an analytical solution for a clamped-edge bimorph disk-type piezoelectric transformer was established by Chen *et al.* (2022). Malikan and Eremeyev (2020) evaluated the nonlinear bending of a piezoflexomagnetic strain gradient nanobeam based on an analytical-numerical solution. Malikan (2017), Malikan and Eremeyev (2021) examined the electromechanical and flexomagnetic buckling of piezoelectric modified couple stress nanoplate based on simplified first-order shear deformation theory and nonlinear strains of Von-Karman. Gia *et al.* (2022) predicted the size-dependent nonlinear vibration of functionally graded composite micro-beams reinforced by carbon nanotubes with piezoelectric layers in thermal environments.

In recent years there has been a huge utilization of numerical methods in analyzing or designing structures due to their relatively low cost and the advanced technology of their software. The finite elements method (FEM) is one of these numerical methods, which is based on dividing the structure into a finite number of small elements and solving each element alone (Asiri *et al.* 2020), then assembling all element solutions to get a solution to the whole structure. FEM has some software, including ANSYS, ABAQUS, COMSOL, and many others. Making use of finite element software to develop or analyze piezoelectric structures has been used extensively and showed very acceptable results when compared to experiments. Lerch *et al.* (1988, 1990) developed a finite element method to analyze the response of a piezoelectric transducer, having a random shape, against vibration from the ambient environment. Their model achieved good agreement with analytical and experimental results. Wang (2004) created a 2D FEM of a piezoelectric bimorph structure to study it statically and dynamically to predict its' mechanical and electrical responses. The generated model produced predictions that are in good agreement with another 3D finite element model for bimorph structures of PVDF and PZT. Ramegowda *et al.* (2020a) investigated the interaction between the piezoelectric layers and the metal layer located in the middle of a thin piezoelectric bimorph structure using FEM. Ali *et al.* (2022) studied the effects of the bonding layer on the performance of piezoelectric actuator considering viscoelastic material as a bonding layer. Bendine *et al.* (2017) introduced a methodology for dealing with ANSYS software to model and active vibration control of a functionally graded material (FGM) plate with piezoelectric layers glued on both sides of the surface. Ramegowda *et al.* (2020b) projected a FEM to study the performance and the fluid-solid interaction of a bimorph piezoelectric structure submerged in fluid, then studied the sensor and actuating effects of the piezoelectric structure. Alnujaie *et al.* (2020) studied forced vibration of a functionally graded porous beam resting on viscoelastic foundation by using finite element method. Akbaş (2020) exploited the Ritz method to investigate the dynamic responses of laminated beams under a moving load in thermal environment. Malekzadeh *et al.* (2022) studied buckling and vibration analysis of a double-layer graphene sheet coupled with a piezoelectric nanoplate.

Recently piezoelectric phenomena have been utilized in operating remotely wireless devices as energy harvesters (Moory-Shirbani *et al.* 2018, Mohammad and Dehghani 2022), where they convert vibrations from ambient environments to electrical energy (Alaei 2016, Nadeem *et al.* 2022). Based on analytical solutions, Erturk and Inman (2008, 2009) developed analytical models based on the Euler-Bernoulli beam theory to investigate the dynamic response of unimorph/bimorph piezoelectric structure and validated their models' with experimental results. Bonello and Rafique (2011) provided two alternative techniques to model energy harvesting

beams, where the first model is an innovative model based on the dynamic stiffness method, and the other is based on the Euler-Beam model. Lin *et al.* (2021) studied the energy harvesting response of a bimorph piezoelectric composite harvester to reveal new insights into the transformation abilities of piezoelectric energy harvester (PEH) from mechanical energy to electrical energy analytically and then validated experiments. Wang *et al.* (2022) designed a uniform stress-distributed bimorph PEH analytically utilizing the Euler-Bernoulli beam model and taking ARC mechanical stopper into account the design. The design was manufactured and examined to achieve nearly two times the voltage compared to the model with only a point stopper. Asthana *et al.* (2020) compared the result of an analytical model extracted from the Euler-Bernoulli model of cantilever PEH against the FEM taking a deflection, output power, and output voltage as the criteria of the comparisons. They found that the difference between the models is only about 6%.

Other works based entirely on the numerical solution method, mainly FEM, in investigating piezoelectric energy harvesters, including Machu *et al.* (2021), designed piezoelectric cantilever beams as energy harvester using different piezoelectric materials in various configurations. Khalatkar *et al.* (2011) developed a 3D FEM of a cantilever piezoelectric energy harvester to study the effects of different geometrical configurations on the output voltage of the harvester, considering different lengths and widths. They expanded their study to account for the effects of different positions of piezoelectric patches along the middle host structure. Their outcomes included that width has a positive relation with voltage output, the length of piezoelectric patches should be half of the total length of the middle host structure, and the best position for maximum voltage output is at the middle of the structure. Benjeddou (2015) presented theoretical and numerical assessments of approximate evaluations and simplified analyses of piezoelectric structures' transverse shear modal effective electromechanical coupling coefficient. Hasan *et al.* (2022) developed two bimorph piezoelectric energy harvester's finite element models, trapezoidal and triangular, comparing them considering natural frequency to reveal that the triangular model has generated higher voltage than the trapezoidal one at resonance frequencies. The reason behind selecting triangular and trapezoidal shapes is that the resonance peak of the harvester is sensitive to variations in geometric dimensions and shape Hosseini and Hosseini (2016). Bhaskar and Thakur (2019) exploited a geometrically nonlinear finite element model for the analysis of laminated plates using a new plate theory. Khazaei *et al.* (2022) conducted a holistic study using the stochastic-excitation high-order-shear-deformation finite element method, studying the contact layer effects on the resulted in harvested power, then parametric studies were conducted to investigate the optimum load-frequency; their outcomes recommended to consider bonding layer to get a more accurate estimation of the resulted power. Jiang *et al.* (2022) developed and compared two models of piezoelectric vibration energy harvesters (PVEH), L-shaped and U-shaped, via COMSOL simulation. With 0.1 g acceleration and different gravity angles and clamping angles, two PVEHs are experienced to find the suitable angle for higher output power. Haldkar *et al.* (2022) produced a 3D finite element model in ANSYS to analyze the behavior of piezoelectric energy harvester with porous piezoelectric patches against different configurations such as the porosity, proof mass position along the extractor, and different load since the resulted in electrical potential is the criteria of the study. Ramegowda *et al.* (2022) developed a mathematical and finite element model of a flexible piezoelectrical energy harvester and compared its' outcomes to experimental results, and decent agreement was found. Phung *et al.* (2022) studied the static bending and free vibration analysis of two-layer variable thickness plates with shear connectors by using FEM.

The effectiveness of nanoscale and surface properties on static and free vibrations conditions of perforated piezoelectric is one of the natural development of studies on the piezoelectric structure and piezoelectrical energy harvester due to the enhancements that can be provided to the structure reducing weight and material needed while achieving the same or even better performance. Adding perforated structures can provide desired behavior, especially in the case of fluid-structure interaction. Luschi and Pieri (2014) established a mathematical solution of equivalent bending and shear of perforated beams when they are under resonance frequencies utilizing the most common equations of Euler-Bernoulli and of shear. They validated their analytical model to finite element model and experimental study, where they achieved great results. Eltahir *et al.* (2018, 2019) extended the analytical work of Luschi and Pieri (2014) by studying nanobeams with square perforations behavior under resonance frequencies considering shear, bending, mass, and rotary inertia as the criteria of the study; the results were validated numerically too after also investigating the effects of perforations' size, number, and length scale parameter on the natural frequency of perforated nanobeams. Silva *et al.* (2016) exploited the wave finite element method in passive vibration control of periodic structures. Eltahir *et al.* (2020a, b) extended the previous work by investigating analytically piezoelectric nanobeams with square perforations response toward nanoscale and surface energy. Considering bending and resonance frequency, they developed their model utilizing different theories such as the nonlocal differential elasticity, the Gurtin-Mudoch model, Hamilton's principles, and the finite element method. Concluding that surface stresses affect more with nanometer thicknesses. Melaibari *et al.* (2022) studied the effect of flexoelectricity on the dynamic response of piezoelectrically layered perforated non-local strain gradient nanobeam. Shevtsova *et al.* (2016) investigated the enhancements resulting from utilizing perforated (porous) piezoelectric ceramics on transducers submerged in water using a Pareto-based approach. They conducted their study developing finite element models in COMSOL linked to MATLAB of two devices, a multilayered projector and a membrane-hydrophone, having porous piezoelectric elements. Mechkour (2022) computed a 3D mathematical model to predict the effects of perforations' dimensions on perforated piezoelectric plates' performance and extended the work to include the effects of the plate's thickness on the plate's deformations and plate's electric potential. Su *et al.* (2019) developed an entirely finite element model studying the effects of perforations on piezoelectric cantilever energy harvester performance, focusing on the size of perforations and their locations throughout the piezoelectric cantilever energy harvester. Their main finding is that perforation has positive effects on voltage output. Anand *et al.* (2021) examined different bimorph cantilever piezoelectric energy harvester structures to decide the optimum design of PEH of ventilation systems. Their findings include rectangular PEH has performed better than the tapered one, and structures with many perforations produced higher voltage and distributed the stress in a better manner. Almitani *et al.* (2019) introduced a semi-analytical model and investigated the dynamic behavior of the perforated beam structure beneath free and forced conditions. Kaur *et al.* (2020) emphasized the effectiveness of the perforations on the piezoelectric energy harvester by studying a perforated rectangular-shaped cantilever piezoelectric and perforated trapezoidal piezoelectric experimentally, and the results showed that the power is higher in the rectangular-shaped cantilever than the trapezoidal one. Assie *et al.* (2021) found that the perforation parameters have a significant impact on the dynamic response of perforated beams under moving loads; raising the perforation filling ratio reduces system flexibility, resulting in lower values of dynamical displacements. Abdelrahman *et al.* (2023) emphasized that the electromechanical and mechanical dynamic response of piezoelectrically layered perforated nanobeams is significantly affected by perforation design and parameters. The

geometrical characteristics of the perforation arrangement might be used to influence either electromechanical or mechanical vibration behaviors.

This work is an extension of our previous works to investigate the effects of different configurations of perforation on the dynamic behavior of piezoelectric bimorph energy harvesters. Focusing on the perforation’s shape, dimension, and distribution throughout the structure, in addition to the effect of the thickness of piezoelectric patches on the performance of the perforated energy harvester. All the models developed are numerical models created on FEM software ANSYS but preceded with mathematical explanations of geometrical and physical aspects of the proposed structures.

2. Mathematical formulation

It is essential to explore and examine the electrostatic and electrodynamic responses of the piezoelectric smart materials structure because of how widely they are used in contemporary control technologies. Considering the perforated bimorph piezoelectric cantilever with top and bottom layers made of the piezoelectric materials having thickness h_p , and the mid-layer is a non-piezoelectric material with thickness h_s and the same length L and width W . The whole thickness of the bimorph structure will be $h = h_s + 2h_p$. The orientation of the polarization of the piezoelectric layers is in the thickness direction. The following equations describe the physical aspects of the structure.

2.1 Equivalent geometrical model

According to the symmetrical square’s perforations pattern, the comparable geometrical variables are derived. As from Fig. 1, the spatial period is taken as l_s , the hollow side is $l_s - t_s$, and the number of holes across the beam in the section is N . It is possible to represent the perforation filling ratio as Melaibari *et al.* (2022)

$$\alpha = \frac{t_s}{l_s} \quad 0 \leq \alpha \leq 1, \quad \alpha = \begin{cases} 0 & \text{Fully perforated} \\ 1 & \text{Fully filled} \end{cases} \quad (1)$$

The equivalent of beam bending and shear stiffness of perforated beams are

$$\frac{(EI)_{eq}}{(EI)_s} = \left\{ \frac{\alpha(N + 1)(N^2 + 2N + \alpha^2)}{(1 - \alpha^2 + \alpha^3)N^3 + 3\alpha N^2 + (3 + 2\alpha - 3\alpha^2 + \alpha^3)\alpha^2 N + \alpha^3} \right\} \quad (2a)$$

$$\frac{(GA)_{eq}}{(EA)_s} = \left(\frac{(1 + N)\alpha^3}{2N} \right) \quad (2b)$$

Where respectively, $(EI)_{eq}$, $(EI)_s$, are the equivalent bending stiffnesses of solid and perforated beams. The equivalent shear stiffnesses of the solid and perforated beams, in turn, are $(GA)_{eq}$, $(GA)_s$. The equivalent initial moment of inertia $(\rho I)_{eq}$ and mass per unit length $(\rho A)_{eq}$ are

$$\frac{(\rho A)_{eq}}{(\rho A)_s} = \left\{ \frac{[(1-N)(\alpha-2)]\alpha}{N+\alpha} \right\} \quad (3a)$$

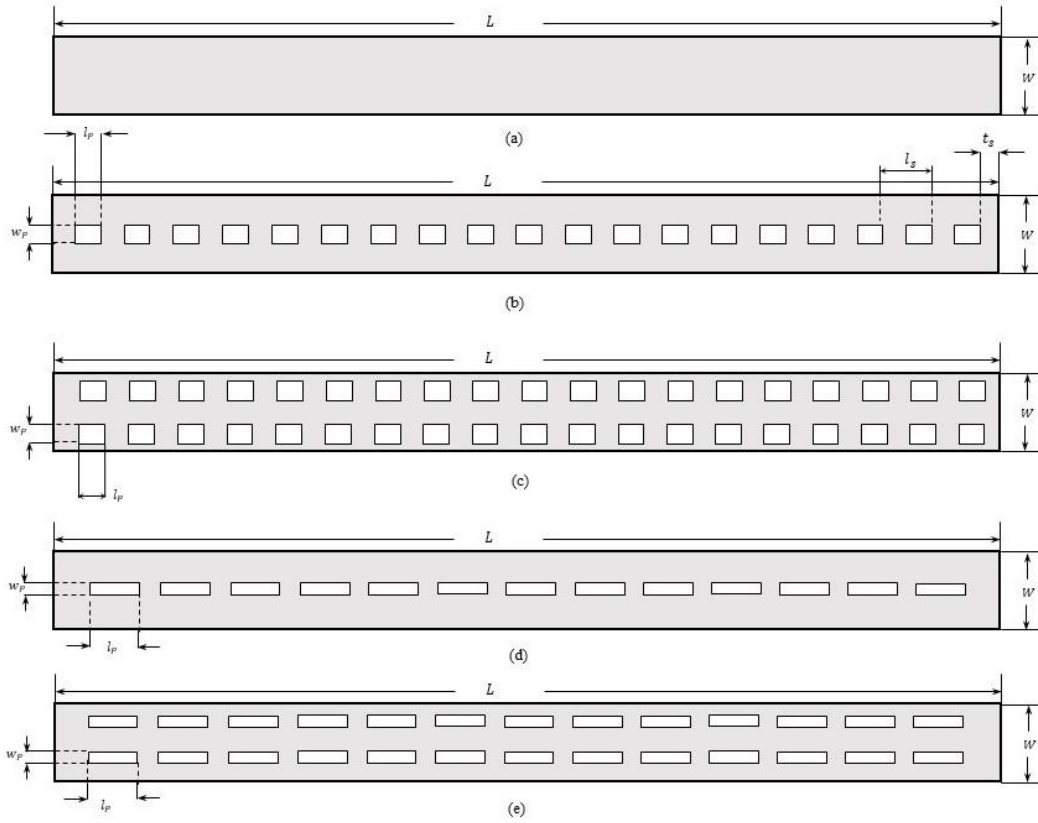


Fig. 1 A schematic of each model of the ten models. Each schematic represents two models: One with 3 mm total thickness and the other with 6 mm total thickness

$$\frac{(\rho I)_{eq}}{(\rho I)_s} = \left\{ \frac{\alpha[(2-\alpha)N^3 + 3N^2 - 2(\alpha-3)(\alpha^2 - \alpha + 1)N + \alpha^2 + 1]}{(N+\alpha)^3} \right\} \quad (3b)$$

2.2 Constitutive equations

Bearing in mind the relation between electric displacement and electric field, l is defined as follows

$$D = \varepsilon E \quad (4)$$

Where D , E , and ε represent the electric displacement, electric field, and dielectric permittivity of the material, respectively. On the other hand, Hook's law defines the relationship between mechanical strain (S) and stress (T) in one direction

$$S = sT \quad (5)$$

Where s indicates the elastic compliance of the material.

The governing equation for the direct piezoelectric effect included two boundary conditions that can be derived from Eq. (4) by adding additional terms to represent mechanical displacement Alaei (2016), as follows

When the piezoelectric material is under a “free” condition, “free” means the ability of the material to change its’ dimensions freely according to the applied field. This is the normal condition (Constant stress condition). The governing equation will be as follows

$$D = dT + \varepsilon^T E \tag{6}$$

Where d is the piezoelectric matrix (charge density per applied stress), ε^T is the permittivity at constant stress T .

When the piezoelectric material is under clamped conditions, “clamped” the governing equation will be as follows

$$D = eS + \varepsilon^S E \tag{7}$$

Where e is the piezoelectric matrix (charge density per strain), ε^S is the permittivity at constant strain.

The governing equation for the indirect piezoelectric effect included two boundary conditions that can be derived from Eq. (5) by adding additional terms to represent electrical displacement Alaei (2016), as follows

Piezoelectric material short-circuited (constant electric field)

$$S = s^E T + dE \tag{8}$$

$$T = c^E S - eE \tag{9}$$

Piezoelectric material open circuit (constant charge density)

$$S = s^D T + gD \tag{10}$$

$$T = c^D S - gD \tag{11}$$

Where s^D and c^D are the elastic compliance and stiffness constant under a constant electric field, and g is the piezoelectric coefficients.

Once the direct effect of piezoelectric material properties is taken into consideration, the form of equations (8) and (9) can be expressed in matrix form

$$\begin{bmatrix} S_1 \\ S_2 \\ S_3 \\ S_4 \\ S_5 \\ S_6 \end{bmatrix} = \begin{bmatrix} s_{11}^E & s_{12}^E & s_{13}^E & s_{14}^E & s_{15}^E & s_{16}^E \\ s_{21}^E & s_{22}^E & s_{23}^E & s_{24}^E & s_{25}^E & s_{26}^E \\ s_{31}^E & s_{32}^E & s_{33}^E & s_{34}^E & s_{35}^E & s_{36}^E \\ s_{41}^E & s_{42}^E & s_{43}^E & s_{44}^E & s_{45}^E & s_{46}^E \\ s_{51}^E & s_{52}^E & s_{53}^E & s_{54}^E & s_{55}^E & s_{56}^E \\ s_{61}^E & s_{62}^E & s_{63}^E & s_{64}^E & s_{65}^E & s_{66}^E \end{bmatrix} \begin{bmatrix} T_1 \\ T_2 \\ T_3 \\ T_4 \\ T_5 \\ T_6 \end{bmatrix} + \begin{bmatrix} d_{11} & d_{21} & d_{31} \\ d_{12} & d_{22} & d_{32} \\ d_{13} & d_{23} & d_{33} \\ d_{14} & d_{24} & d_{34} \\ d_{15} & d_{25} & d_{35} \\ d_{16} & d_{26} & d_{36} \end{bmatrix} \begin{bmatrix} E_1 \\ E_2 \\ E_3 \end{bmatrix} \tag{12}$$

$$\begin{bmatrix} D_1 \\ D_2 \\ D_3 \end{bmatrix} = \begin{bmatrix} d_{11} & d_{12} & d_{13} & d_{14} & d_{15} & d_{16} \\ d_{21} & d_{22} & d_{23} & d_{24} & d_{25} & d_{26} \\ d_{31} & d_{32} & d_{33} & d_{34} & d_{35} & d_{36} \end{bmatrix} \begin{bmatrix} T_1 \\ T_2 \\ T_3 \\ T_4 \\ T_5 \\ T_6 \end{bmatrix} + \begin{bmatrix} \varepsilon_{11}^T & \varepsilon_{12}^T & \varepsilon_{13}^T \\ \varepsilon_{21}^T & \varepsilon_{22}^T & \varepsilon_{23}^T \\ \varepsilon_{31}^T & \varepsilon_{32}^T & \varepsilon_{33}^T \end{bmatrix} \begin{bmatrix} E_1 \\ E_2 \\ E_3 \end{bmatrix} \tag{13}$$

Considering the piezoelectric structure in general as piezoelectric materials with the ability to be poled in only one direction, mainly the thickness direction of the material, and generalizing

isotropic properties for piezoelectric material, the linear constitutive equations can be written, according to the ANSI/IEEE Standard 176-1987, as follows Meeker (1996)

$$\begin{bmatrix} S_1 \\ S_2 \\ S_3 \\ S_4 \\ S_5 \\ S_6 \end{bmatrix} = \begin{bmatrix} s_{11}^E & s_{12}^E & s_{13}^E & 0 & 0 & 0 \\ s_{21}^E & s_{22}^E & s_{23}^E & 0 & 0 & 0 \\ s_{31}^E & s_{32}^E & s_{33}^E & 0 & 0 & 0 \\ 0 & 0 & 0 & s_{44}^E & 0 & 0 \\ 0 & 0 & 0 & 0 & s_{55}^E & 0 \\ 0 & 0 & 0 & 0 & 0 & s_{66}^E \end{bmatrix} \begin{bmatrix} T_1 \\ T_2 \\ T_3 \\ T_4 \\ T_5 \\ T_6 \end{bmatrix} + \begin{bmatrix} 0 & 0 & d_{31} \\ 0 & 0 & d_{32} \\ 0 & 0 & d_{33} \\ 0 & d_{15} & 0 \\ d_{15} & 0 & 0 \\ 0 & 0 & 0 \end{bmatrix} \begin{bmatrix} E_1 \\ E_2 \\ E_3 \end{bmatrix} \quad (14)$$

$s_{66}^E = 2(s_{11}^E - s_{12}^E)$

3. Finite element formulation

The methodology of Finite Element FE is to discretize the beam domain into numbers of elements and derive the plate theory equations of motions for each element. Based on Hamilton's principle. For all conceivable pathways, the overall energy variance from 0 to t_0 is zero Khazaei et al. (2022)

$$\delta \int_0^{t_0} [(K.E. - P.E. + W_{el}) + W_E] dt = 0 \quad (15)$$

$K.E.$ = kinetic energy, $P.E.$ = Potential energy, W_{el} = electrical energy, W_E = external mechanical force.

By defining the kinetic and potential energies for piezoelectric and non-piezoelectric domains and outer mechanical forces, Eq. (15) can be expressed as

$$\delta \int_0^{t_0} \left[\overbrace{\iiint \rho \delta r^t \dot{r} dt dV}^{K.E.} - \overbrace{\iiint \rho \delta \varepsilon^t \sigma dV}^{P.E.} + \overbrace{\iiint \rho \delta \varepsilon^t e^t E dV_p} + \overbrace{\iiint \delta E^t e \varepsilon dV_p}^{W_{el}} + \overbrace{\iiint \delta E^t e D dV_p}^{W_E} + \overbrace{\delta r f_E dt} \right] \quad (16)$$

Where ρ : density, r : mechanical displacement field, ε : strain, σ : stress, f_E : external force, e : piezoelectric factor, E : electric field, D : electric displacement field.

The mathematical expressions of piezoelectric beams attached to a resistance load \mathbb{R} are

$$\begin{aligned} [m^e] \{\ddot{\chi}^e\} + [c_a^e] \{\dot{\chi}^e\} + ([k_{qq}^e] + j[c_s^e]) \{\chi^e\} - [k_{q\phi}^e] v_e &= f_E \\ [k_{q\phi}^e]^t \{\dot{\chi}^e\} + \frac{v_e}{R} + k_{\phi\phi}^e v_e &= 0 \end{aligned} \quad (17)$$

$\{\chi^e\} \in \mathbb{R}^{6 \times 1}$: mechanical degrees of freedom for each element, $v_e \in \mathbb{R}$: the electrode-to-electrode potential differential, $[m^e] \in \mathbb{R}^{6 \times 6}$: composition of the mass matrix of the elements, $[k_{qq}^e] \in \mathbb{R}^{6 \times 6}$: composition of the stiffness matrix of the elements, $[k_{q\phi}^e] \in \mathbb{R}^{6 \times 1}$: Electromechanical coupling matrix element, $[c_a^e] \in \mathbb{R}^{6 \times 6}$: The viscous damping matrix of the element, $[c_s^e] \in \mathbb{R}^{6 \times 6}$: matrix of structural damping elements.

4. Design and material properties

If the piezoelectric layer is mounted on one side of the substrate, it is called an unimorph structure, and if the piezoelectric layers are mounted on both sides of the substrate, it is called a bimorph structure. The finite element method (FEM) is applied using the commercial package ANSYS APDL 2021. Fig. 1 illustrated the dimensions of the bimorph cantilevers models. The models are composed of two layers of PZT 3195HD and sandwiched metallic brass. The bonding layers between piezoelectric patches and the sandwiched metal are neglected, assuming perfect bonding.

The models used in this study consist of, firstly, two solid models (without holes) having the same length and width but different thicknesses. The first model has a thickness of 1mm for each part of the bimorph structure, and the second one has a thickness of 2 mm for each part of the bimorph structure, illustrated in Fig. 1(a). Secondly, another two models with the same length, width, squared perforations, and perforations' dimensions, but the difference is that one of the two models has one row of perforations, and the other has two rows of perforations shown in Fig. 1 (b) and (c). These two models are also created twice, the first time with a total thickness of 3 mm (each part has 1 mm thickness) and the second time with a 6 mm total thickness (each part has 2 mm thickness) to get four models of squared perforation PEH. Lastly, the previous four models are recreated again but with rectangular perforations, as shown in Fig. 1 (d) & (e), to have in total of ten models, which will result in clearer comparison and findings.

Square perforated models have 6.25 mm×6.25 mm for square holes' dimensions repeated 19 squares per row, while rectangular perforation models have 3.125 mm×12.5 mm for rectangular pit dimensions repeated 13 times per row. Dimensions of the perforations are based on the ratio of the perforation presented in Asthana *et al.* (2020), with a filling ratio of 75%, and the remaining ratio is 25%. Considering rectangular and square shapes, which are the most common perforation shapes. The dimensions are calculated to get a symmetry shape along the x and y axes and to have a more regular shape for the entire system. With the expansion of additive manufacturing technologies (3D printing), a lot of work has been done in producing piezoelectric devices additively Chen *et al.* (2016), Cui *et al.* (2019), Cholleti (2018), with this in mind, various complex shapes can be studied including a perforated piezoelectric structure, as proposed in this work. The structure in this study is also large enough to be produced using subtractive manufacturing methods, water jet cutting, or laser cutting, Almitani *et al.* (2019) investigated the dynamic performance of a perforated beam structure under free and forced conditions; thus, the present perforated model is mandatory in some applications like heat exchangers, nuclear plants, filtration, and microelectromechanical systems (MEMS). Also, by referring to Kaur *et al.* (2020) work, this model could be used in wireless structural health monitoring and so on.

The 20-node coupled SOLID226 element is used to represent the piezoelectric material, while the 20-node SOLID186 structural element is selected to represent the metallic sandwiched (Brass) material, and the CIRCU94 element is added to account for electric resistance through the models. For the solid models (without perforations), the elements in each mesh model are 540 for the solid model with a thickness of 3 mm and 1170 with 6 mm of thickness for the perforated structures meshed with an element size of 2 mm. The overall number of elements created is 4686 for the model with 1 row of square perforations and 3 mm of thickness, 4710 for the model with 1 row of square perforations and 6 mm of thickness, 4758 for the both of 3 and 6 mm thickness model with two rows of square perforations, 4878 for the both of 3 and 6 mm thickness model with 1 row of rectangular perforations, 3890 for the both of 3 and 6 mm thickness model with two rows of

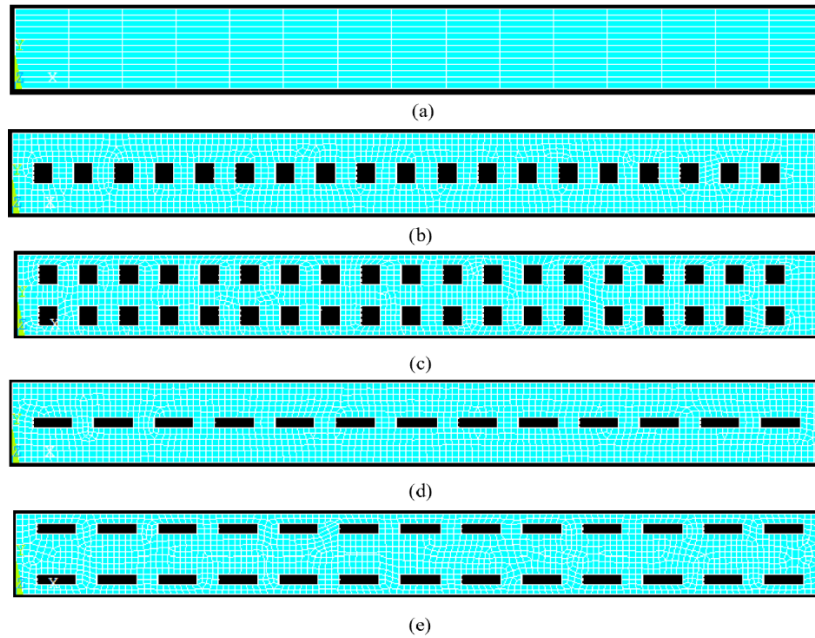


Fig. 2 Meshed models. (a) solid models, (b) Square perforations with one-row models, (c) Square perforations with two rows models, (d) Rectangular perforations with one-row models, and (e) Rectangular perforations with two rows models

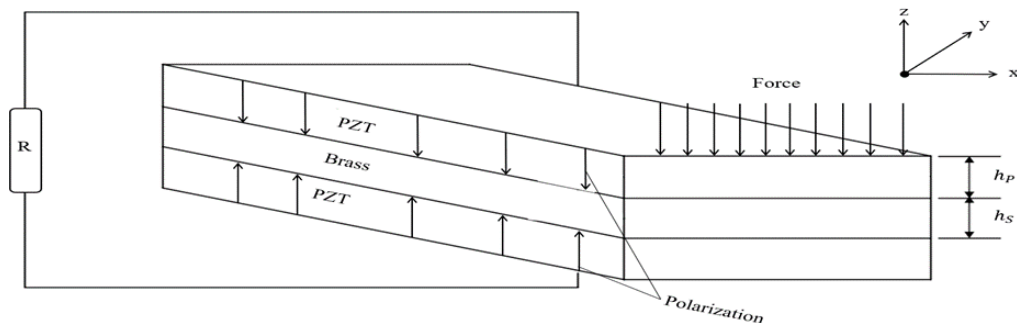


Fig. 3 A bimorph piezoelectric harvester with clamped-forced boundary conditions

rectangular perforations, meshed models are demonstrated in Fig. 2.

PZT 3195HD and substrate material properties are taken from Hasan *et al.* (2022), geometry dimensions are taken from Shevtsova *et al.* (2016) but taking equal length for the piezoelectric patches and the brass structure, which is the commonly used configuration of bimorph energy harvester, Ramegowda *et al.* (2020b), Ali *et al.* (2022), Khalatkar *et al.* (2011), Jiang *et al.* (2022), illustrated in Table 1. Two types of analyses are under focus, starting with modal analysis to extract the natural frequencies of each model and the corresponding modal shapes, and then dynamic analysis (mainly harmonic analysis) to study the performance of the models under certain boundary conditions, Fig. 3 shows the boundary conditions governing the models.

The following model is applicable for thin and moderated thick structures with one-

Table 1 Geometric parameters and mechanical properties

Dimensions and material properties	
Sandwiched Material	Metallic Brass
Youngs Modulus (GPa), E_s	100
Poisson's ratio	0.307
Density (kgm^3), ρ_s	8780
Brass sheet dimensions Models' (mm^3) ($L * W * h_s$)	250 * 25 * 1 or 2
Piezoelectric Material	PZT 3195HD
Youngs Modulus (GPa), E_p	111
Stiffness Constants (GPa)	
$s_{11}^E = s_{22}^E$	15.1
s_{12}^E	-4.8
$s_{13}^E = s_{23}^E$	-7.6
s_{33}^E	-18.6
s_{44}^E	40.0
s_{55}^E	40.0
s_{66}^E	39.8
Piezoelectric Constants ($\frac{\text{m}}{\text{V}} * 10^{-12}$)	
d_{31}	-190
d_{33}	390
d_{15}	460
Relative dielectric constants	
$\epsilon_{11}^T = \epsilon_{22}^T$	1900
ϵ_{33}^T	1600
Density (kgm^3), ρ_p	7800
Piezoelectric parts dimensions (mm^3) ($L * W * h_p$)	250 * 25 * 1 or 2

dimensional electric field. However, the solid structure with 3D polarization cannot be considered in this study.

5. Validation

In this section, the results of the triangular tapered developed by Hasan *et al.* (2022) will be used to validate the method used in developing the perforated bimorph piezoelectric energy harvester finite element models on the commercial package ANSYS APDL 2021. The regenerated model of Hasan *et al.* (2022), following the method, achieved the exact agreement of the original model of Hasan *et al.* (2022), considering resonance frequencies. Fig. 4 shows the validation of the regenerated FE triangular model with the original model of Hasan *et al.* (2022).

The results of harmonic analysis of the regenerated model of triangular tapered disclosed very good agreement with the results of Hasan *et al.* (2022), with maximum tip displacement in conjunction with 1200 Ω resistance, 0.24 N harmonic load, and frequency range of 200 Hz to 500 Hz, is found as 61.66 mm, which is close to 61.74 mm found by Hasan *et al.* (2022).

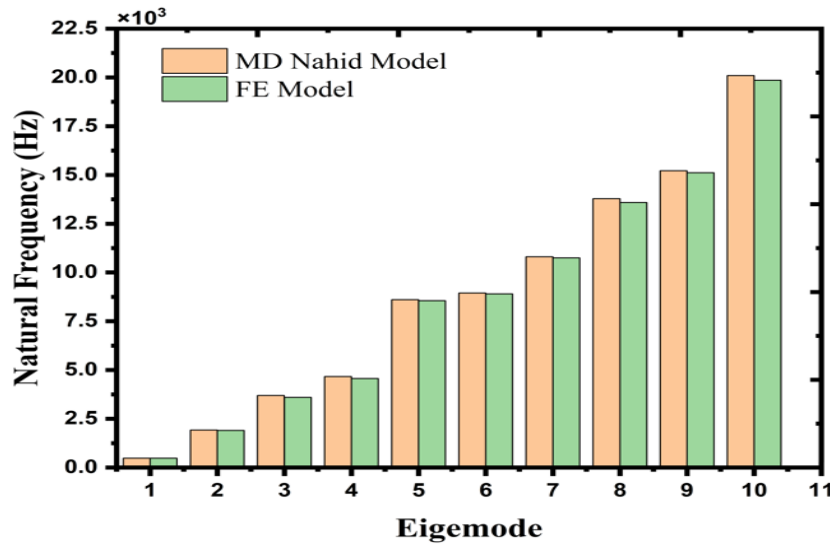


Fig. 4 Validation of the FE model constructing process

6. Results and discussion

In this study, the thickness of piezoelectric elements, perforation shape, and the number of perforated rows are set as the parameters for investigating the bimorph piezoelectric energy harvester performance taking resonance frequency and output voltage as the criteria of this parametric study. Natural frequencies can be calculated using the developed finite element model in ANSYS by conducting Modal analysis. The output voltage can be obtained from Harmonic analysis with sufficient boundary conditions.

6.1 Modal analysis:

Studying the characteristic frequencies is important as piezoelectric energy harvesters are designed to collect vibration energy at these frequencies as it will result in the maximum voltage output. In modal analysis, all the models agreed on achieving higher natural frequency when the thickness increased from 3 mm to 6 mm. In fact, as illustrated in Table 3, all 6 mm models achieved nearly double the frequency of 3 mm models in all cases with perforations and without perforations for the first five natural frequencies. For the remaining five natural frequencies, the difference decreased to only a third. However, naturally increasing the thickness should increase the mass, resulting in the reduction of the natural frequencies, as mass and natural frequency have a negative relationship. But on the other hand, the stiffness of the structure will rise with the increase of the thickness leading to elevating the natural frequency, as stiffness has a positive relationship with a natural frequency. That means the rise in natural frequency resulted from stiffness improvement due to thickness increase has more effect and overpassed the reduction that happened from the increased mass. Figs. 5, 6, and 7 show the first mode shapes of all ten models. However, the results showed good agreement with the work of Almitani *et al.* (2019) in the literature review which they concluded that the increase in the hole number caused a lowering in the natural frequency.

Table 2 The resonance frequencies for models 1 and 2 with different rows and thicknesses for each case

Mode Frequency (Hz)	Solid Model 3 mm	Solid Model 6 mm	Square Perforations Models				Rectangular Perforations Models			
			With one row		With two rows		With one row		With two rows	
			h (3 mm)	h (6 mm)	h (3 mm)	h (6 mm)	h (3 mm)	h (6 mm)	h (3 mm)	h (6 mm)
1	23.928	47.696	22.179	44.089	20.07	39.604	23.353	46.587	22.942	45.693
2	145.56	199.75	135.31	206.91	123.22	177.19	141.97	205.04	139.59	185.57
3	199.68	289.93	206.68	268.8	176.78	243.01	204.83	282.97	185.24	277.74
4	405.88	789.75	376.78	682.48	344.37	626.99	387.12	705.46	388.44	700.79
5	420.17	804.71	377.13	746.96	361.52	677.21	394.98	784.87	391.64	770.49
6	797.85	1197.4	737.39	1185.6	674.29	1024.5	771.4	1179	758.37	1083.7
7	1196.9	1570.3	1137.5	1455.1	1020.8	1321.1	1167.1	1527	1081	1498.4
8	1267.6	2379.9	1183.1	2059.8	1091.6	1893.7	1176.9	2125.4	1180.7	2111.5
9	1331.4	2591.6	1219.6	2394.2	1116.6	2176.4	1274.6	2510	1253.1	2462.8
10	2014.4	3150.5	1820.4	2976.4	1668.2	2586.2	1901.1	2970.6	1868.6	2769.8

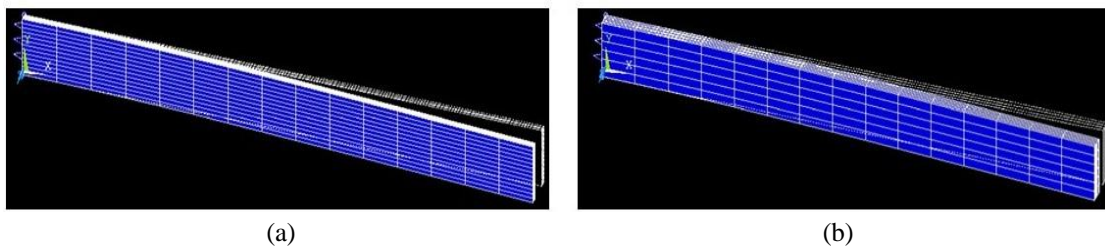


Fig. 5 Deformed shapes of the solid models, (a) $h=3$ mm, (b) $h=6$ mm

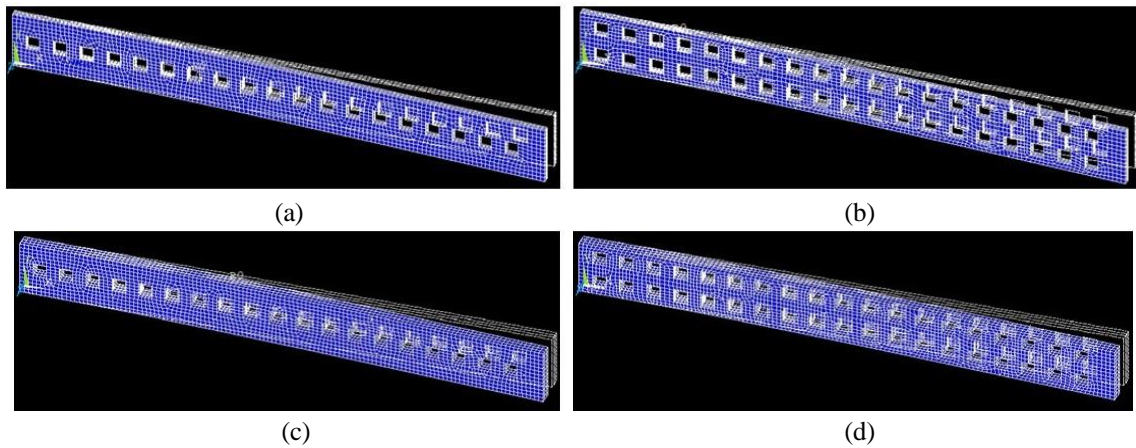


Fig. 6 Deformed shapes of models with square perforations, (a) one row, $h=3$ mm, (b) two rows, $h=3$ mm, (c) one row, $h=6$ mm, (d) two rows, $h=6$ mm

6.2 Harmonic analysis

As the proposed energy harvester collects the energy from vibration, a harmonic (dynamic) analysis is conducted. The boundary conditions in the harmonic analysis are shown in Fig. 3 and

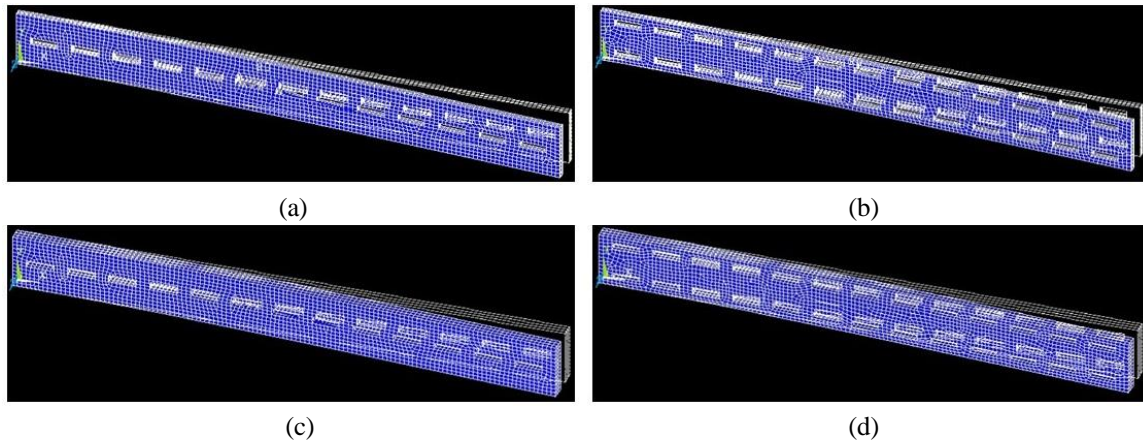


Fig. 7 Deformed shapes of models with rectangular perforations, (a) 1 row, $h=3$ mm, (b) 2 rows, $h=3$ mm, (c) 1 row, $h=6$ mm, (d) 2 rows, $h=6$ mm

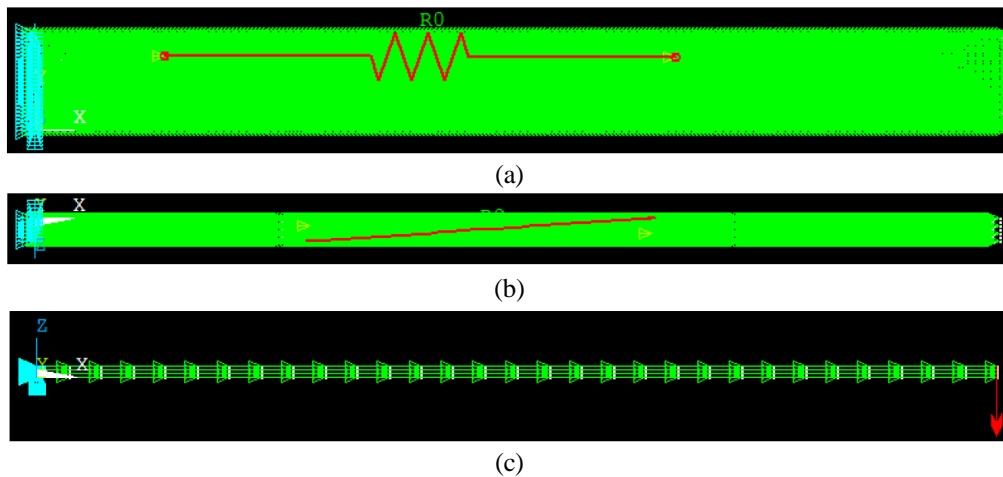


Fig. 8 Meshed model and harmonic analysis boundary conditions, including excitation force and circuit resistance

Fig. 8, where the structure is clamped from one side and free on the other side. A force of 0.24 N is taken to represent the forced excitation, but the value is only for comparison, and assumed, the optimum force can be optimized in later studies. The circuit resistance is also assumed to be 1200Ω .

Firstly, a comparison of the solid models revealed that the modes with the thinner thickness ($h=3$ mm) were able to produce higher electrical potential at the first natural frequency than the thicker model ($h=6$ mm) nearly three times. Fig. 9 illustrates that. This might be induced by the thicker substrate structure and thicker piezoelectric elements resulting in increasing the stiffness of the structure, and the excitation force is not enough to cause high stresses.

Secondly, solid models, when compared to models with perforations squared and rectangular, solid models harvested much less electrical potential. Nearly the models that have a 3 mm thickness with squared and rectangular perforation achieved seven times higher than the solid

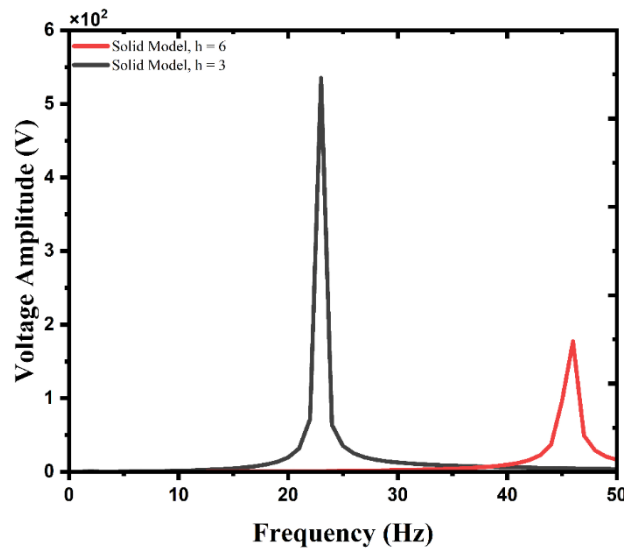


Fig. 9 Resulted in the electrical potential of models without perforations

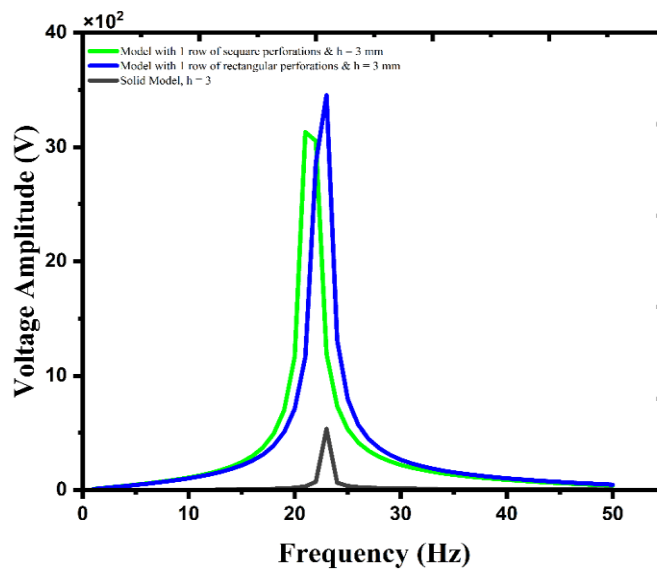


Fig. 10 The performance of the thin perforated models against the thinner solid model

model with the same thickness, as shown in Fig. 10. It is also noticed that the model with rectangular one row of perforations achieved higher output comparing it to the one row of squared perforations model. In Fig. 11, the same phenomena were observed with the models that have 6 mm as thickness and one row of square and rectangular perforations. The square and rectangular perforations with one-row models achieved nearly the same output of voltage but at different resonance frequencies. However, both achieved much higher output than the solid model with the same thickness.

When it comes to the effects of rows, by referring to Fig. 10, the models with one row and 3

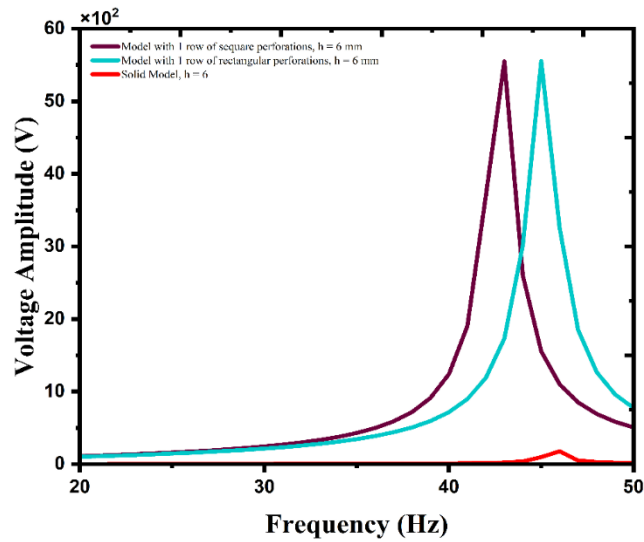


Fig. 11 The performance of the thick perforated models with one row of perforations against the thick solid model

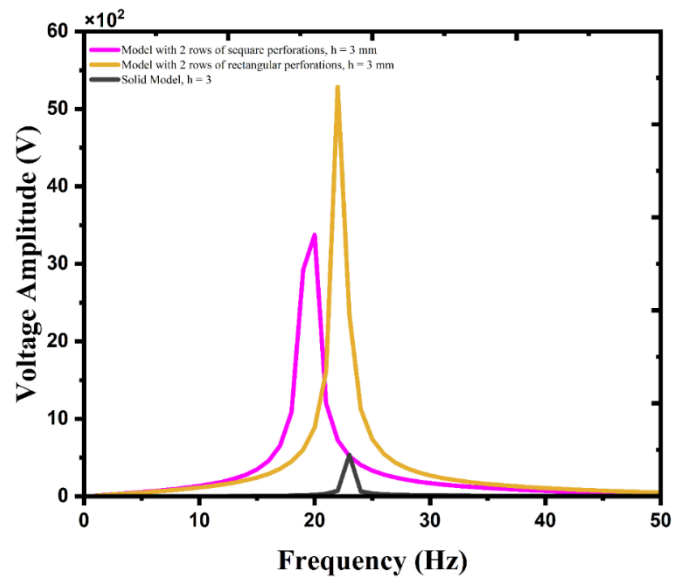


Fig. 12 The performance of the thin perforated models with two rows of perforations

mm of thicknesses and square or rectangular perforations showed fewer achievements in the harvested electrical potential compared to Fig. 12, which showed higher voltage in models with two rows and 3 mm of thicknesses with square and rectangular perforations.

Fig. 13 illustrates the results of the models that have 6 mm of thickness with two rows of square or rectangular perforations, which showed similar results in the voltage output with the models that have 6 mm of thickness with one row of square or rectangular perforations in Fig. 11, but at the different natural frequency.

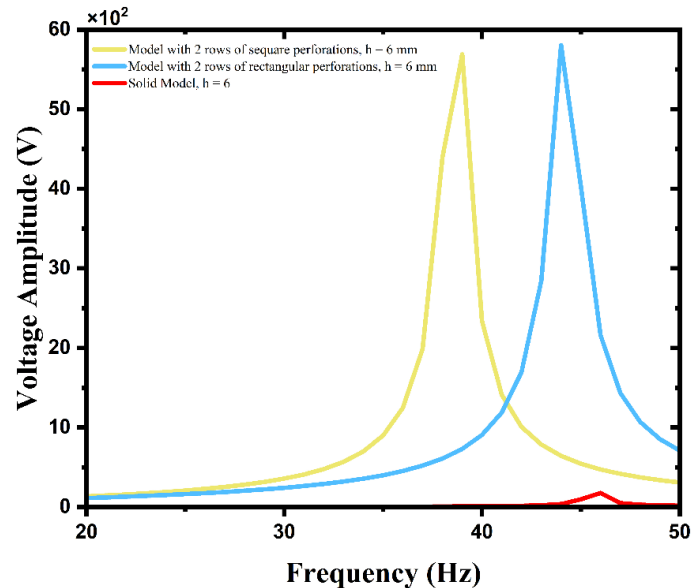


Fig. 13 The performance of the thick perforated models with two rows of perforations

By considering the models with 3 mm of thicknesses in all cases, it is noticed that the rectangular two rows perforated model achieved the higher output of electrical potential among the five models with the same thickness. On the other hand, the solid model with 3 mm of thickness achieved the lowest voltage. During the remaining three models, one row, two rows squared perforated models, and the model with one row of rectangular perforations have the same output at different natural frequencies. Fig. 14 shows these outcomes.

Regarding the models with 6 mm of thickness, all of them except the solid model with the same thickness achieved nearly the same voltage at different natural frequencies. But also, it is observed that the model with two rows of rectangular perforations has the highest electrical potential output. Fig. 15 illustrates the findings of the thick model comparison.

Fig. 16 compares all the models together (3 mm and 6 mm of thickness), with and without perforations, rectangular perforations, and square perforations, and one row or two rows of perforations shows that the models with 6 mm of thickness always achieved the highest voltage except for the solid models which is the lowest one. The model that has 3 mm of thickness with two rows of rectangular perforations accomplished an electrical potential close to the thick models. In contrast, the other with the same thickness of models was able to produce nearly half of the voltage produced by thick perforated models.

The results of this work showed that the electrical potential of output becomes better when the increase of the perforations is synced with the increase in the thickness; referring to the work of Kaur *et al.* (2020), in the literature review, they investigated the effectiveness of the perforations on the electrical potential of output regardless changing the thickness, which resulted in a reduction in the fluttering effect, thus; caused in lesser strain and consequently the power is reduced. Abdelrahman *et al.* (2023) concluded that the perforation configuration and parameters are affecting the electromechanical and mechanical dynamic behavior, thus; the results showed a higher electrical potential of output for the rectangular than square perforation.

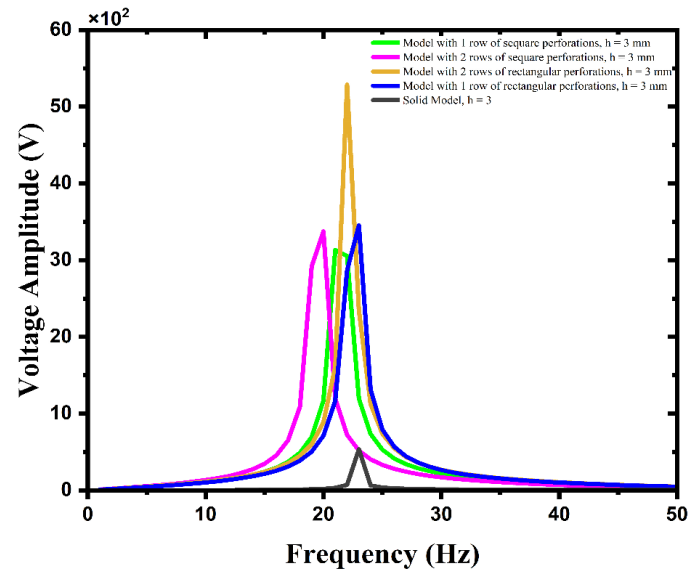


Fig. 14 Comparison of the produced voltage of thin models in all cases

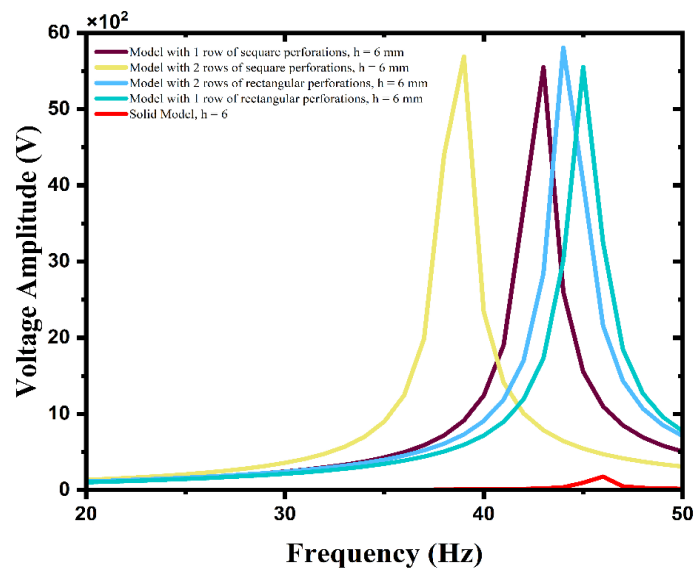


Fig. 15 Comparison of the produced voltage of thin models in all cases

5. Conclusions

The conducted parametric study investigating the effects of perforations shape and number and the effect of structure's thickness on the output of the bimorph cantilever piezoelectric energy harvester revealed many outcomes. Firstly, it is noticed that the thickness of the bimorph structure has a positive relationship with the natural frequency of the piezoelectric bimorph cantilever energy harvester as whenever the thickness is increased, the natural frequency increases nearly at

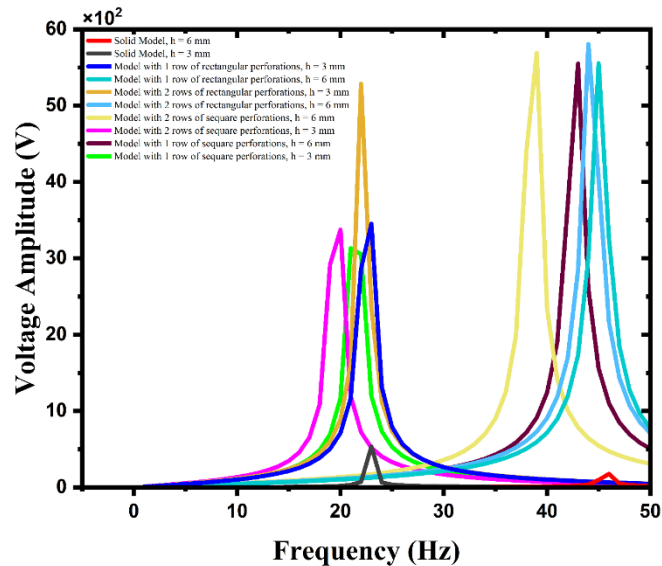


Fig. 16 Compares all the results of the harmonic analyses

the same ratio. Secondly, perforations, no matter their shape, have a positive effect on the produced voltage due to the concentration of stresses. Although that, models with relatively small thickness tend to produce nearly the same electrical potential with rectangular perforations or square perforations of one row, while they produce nearly double with two rows of perforations having a rectangular shape. For thick energy harvesters, the shape of the perforations and the number of perforations does not have much effect on the produced voltage. Lastly, the best perforation shape is found to be the rectangular shape, and optimally they should be in two rows, and thin piezoelectric bimorph energy harvesters can produce nearly the same voltage of harvesters that have twice the thickness by making rectangular perforations in two rows. Refer to the approximate models in the literature investigated by Kaur *et al.* (2020), Assie *et al.* (2021), and Abdelrahman *et al.* (2023), it can be concluded that some benefits in the present model, such as number and shape of perforation greatly effect on the produced voltage and the perforations has a negative relationship with a natural frequency. On the other hand, thickness has a positive relationship with the natural frequency. Perforation has a negative relationship with the stiffness of the structure, which is considered a drawback for the model.

References

- Abdelrahman, A.A., Abdelwahed, M.S., Ahmed, H.M., Hamdi, A. and Eltahir, M.A. (2023), "Investigation of size-dependent vibration behavior of piezoelectric composite nanobeams embedded in an elastic foundation considering flexoelectricity effects", *Math.*, **11**(5), 1180. <https://doi.org/10.3390/math11051180>.
- Akbaş, Ş.D. (2020), "Dynamic responses of laminated beams under a moving load in thermal environment", *Steel Compos. Struct.*, **35**(6), 729-737. <https://doi.org/10.12989/scs.2020.35.6.729>.
- Alaei, Z. (2016), *Power Enhancement in Piezoelectric Energy Harvesting*.
- Ali, I.A., Alazwari, M.A., Eltahir, M.A. and Abdelrahman, A.A. (2022) "Effects of viscoelastic bonding

- layer on performance of piezoelectric actuator attached to elastic structure”, *Mater. Res. Expr.*, **9**(4), 045701. <https://doi.org/10.1088/2053-1591/ac5cae>.
- Almitani, K.H. (2019), “On forced and free vibrations of cutout squared beams”, *Steel Compos. Struct.*, **32**(5), 643-655. <https://doi.org/10.12989/scs.2019.32.5.643>
- Alnujaie, A., Akbas, S.D., Eltahaer, M.A. and Assie, A. (2021), “Forced vibration of a functionally graded porous beam resting on viscoelastic foundation”, *Geomech. Eng.*, **24**(1), 91-103. <https://doi.org/10.12989/gae.2021.24.1.091>.
- Anand, A., Pal, S. and Kundu, S. (2021), “Multi-perforated energy-efficient piezoelectric energy harvester using improved stress distribution”, *IETE J. Res.*, 1-16. <https://doi.org/10.1080/03772063.2021.1913071>.
- Asiri, S.A., Akbaş, Ş.D. and Eltahaer, M.A. (2020), “Dynamic analysis of layered functionally graded viscoelastic deep beams with different boundary conditions due to a pulse load”, *Int. J. Appl. Mech.*, **12**(05), 2050055. <https://doi.org/10.1142/S1758825120500556>.
- Assie, A., Akbaş, Ş.D., Bashiri, A.H., Abdelrahman, A.A. and Eltahaer, M.A. (2021), “Vibration response of perforated thick beam under moving load”, *Eur. Phys. J. Plus*, **136**, 1-15. <https://doi.org/10.1140/epjp/s13360-021-01224-2>.
- Asthana, P. and Khanna, G. (2020) “Characterization and optimization of piezoelectric bimorph cantilever structure for ambient vibration-based energy harvesting application”, *Integr. Ferroelec.*, **211**(1), 45-59. <https://doi.org/10.1080/10584587.2020.1803674>.
- Badr, B.M. and Ali, W.G. (2011), “Applications of piezoelectric materials”, *Adv. Mater. Res.*, **189**, 3612-3620. <https://doi.org/10.4028/www.scientific.net/AMR.189-193.3612>.
- Bendine, K., Boukhoulda, B.F., Nouari, M. and Satla, Z. (2017) “Structural modeling and active vibration control of smart FGM plate through ANSYS”, *Int. J. Comput. Meth.*, **14**(04), 1750042. <https://doi.org/10.1142/S0219876217500426>.
- Benjeddou, A. (2015), “Approximate evaluations and simplified analyses of shear-mode piezoelectric modal effective electromechanical coupling”, *Adv. Aircraft Spacecraft Sci.*, **2**(3), 275. <https://doi.org/10.12989/aas.2015.2.3.275>.
- Bhaskar, D.P. and Thakur, A.G. (2019), “FE modeling for geometrically nonlinear analysis of laminated plates using a new plate theory”, *Adv. Aircraft Spacecraft Sci.*, **6**(5), 409-426. <https://doi.org/10.12989/aas.2019.6.5.409>.
- Bonello, P. and Rafique, S. (2011), “Modeling and analysis of piezoelectric energy harvesting beams using the dynamic stiffness and analytical modal analysis methods”, *J. Vib. Acoust.*, **133**(1), 011009. <https://doi.org/10.1115/1.4002931>.
- Chen, S.E., Gunawan, H. and Wu, C.C. (2022) “An electromechanical model for clamped-edge bimorph disk type piezoelectric transformer utilizing kirchhoff thin plate theory”, *Sensor.*, **22**(6), 2237. <https://doi.org/10.3390/s22062237>.
- Chen, Z., Song, X., Lei, L., Chen, X., Fei, C., Chiu, C.T., ... & Zhou, Q. (2016), “3D printing of piezoelectric element for energy focusing and ultrasonic sensing”, *Nano Energy*, **27**, 78-86. <https://doi.org/10.1016/j.nanoen.2016.06.048>.
- Cholleti, E.R. (2018), “A review on 3D printing of piezoelectric materials”, *IOP Conf. Ser.: Mater. Sci. Eng.*, **455**(1), 012046. <https://doi.org/10.1088/1757-899X/455/1/012046>.
- Cui, H., Hensleigh, R., Yao, D., Maurya, D., Kumar, P., Kang, M.G., ... & Zheng, X. (2019), “Three-dimensional printing of piezoelectric materials with designed anisotropy and directional response”, *Nat. Mater.*, **18**(3), 234-241. <https://doi.org/10.1038/s41563-018-0268-1>.
- Eltahaer, M.A., Abdraboh, A.M. and Almitani, K.H. (2018), “Resonance frequencies of size-dependent perforated non-local nanobeam”, *Microsyst. Technol.*, **24**, 3925-3937. <https://doi.org/10.1007/s00542-018-3910-6>.
- Eltahaer, M.A., Omar, F.A., Abdalla, W.S. and Gad, E.H. (2019), “Bending and vibrational behaviors of piezoelectric non-local nanobeam including surface elasticity”, *Wave. Random Complex Media*, **29**(2), 264-280. <https://doi.org/10.1080/17455030.2018.1429693>.
- Eltahaer, M.A., Omar, F.A., Abdalla, W.S., Kabeel, A.M. and Alshorbagy, A.E. (2020), “Mechanical analysis of cutout piezoelectric non-local nanobeam including surface energy effects”, *Struct. Eng. Mech.*, **76**(1),

- 141-151. <https://doi.org/10.12989/sem.2020.76.1.141>.
- Eltaher, M.A., Omar, F.A., Abdraboh, A.M., Abdalla, W.S. and Alshorbagy, A.E. (2020) "Mechanical behaviors of piezoelectric non-local nanobeam with cutouts", *Smart Struct. Syst.*, **25**(2), 219-228. <https://doi.org/10.12989/sss.2020.25.2.219>.
- Erturk, A. and Inman, D.J. (2008), "On mechanical modeling of cantilevered piezoelectric vibration energy harvesters", *J. Intel. Mater. Syst. Struct.*, **19**(11), 1311-1325. <https://doi.org/10.1177/1045389X07085639>.
- Erturk, A. and Inman, D.J. (2009), "An experimentally validated bimorph cantilever model for piezoelectric energy harvesting from base excitations", *Smart Mater. Struct.*, **18**(2), 025009. <https://doi.org/10.1088/0964-1726/18/2/025009>.
- Gia Phi, B., Van Hieu, D., Sedighi, H.M. and Sofiyev, A.H. (2022), "Size-dependent nonlinear vibration of functionally graded composite micro-beams reinforced by carbon nanotubes with piezoelectric layers in thermal environments", *Acta Mechanica*, **233**(6), 2249-2270. <https://doi.org/10.1007/s00707-022-03224-4>.
- Haldkar, R.K., Cherpakov, A.V., Parinov, I.A. and Yakovlev, V.E. (2022), "Comprehensive numerical analysis of a porous piezoelectric ceramic for axial load energy harvesting", *Appl. Sci.*, **12**(19), 10047. <https://doi.org/10.3390/app121910047>.
- Hasan, M.N., Muktadir, M.A. and Alam, M. (2022) "Comparative study of tapered shape bimorph piezoelectric energy harvester via finite element analysis", *Forc. Mech.*, **9**, 100131. <https://doi.org/10.1016/j.finmec.2022.100131>.
- Hosseini, R. and Hamed, M. (2016), "Resonant frequency of bimorph triangular V-shaped piezoelectric cantilever energy harvester", *J. Comput. Appl. Res. Mech. Eng.*, **6**(1), 65-73. <https://doi.org/10.22061/jcarme.2016.521>.
- Jiang, W., Wang, L., Wang, X., Zhao, L., Fang, X. and Maeda, R. (2022), "Comparison of L-shaped and U-shaped beams in bidirectional piezoelectric vibration energy harvesting", *Nanomater.*, **12**(21), 3718. <https://doi.org/10.3390/nano12213718>.
- Kaur, N., Mahesh, D. and Singamsetty, S. (2020), "An experimental study on piezoelectric energy harvesting from wind and ambient structural vibrations for wireless structural health monitoring", *Adv. Struct. Eng.*, **23**(5), 1010-1023. <https://doi.org/10.1177/1369433219886956>.
- Khalatkar, A., Gupta, V.K. and Haldkar, R. (2011), "Modeling and simulation of a cantilever beam for optimal placement of piezoelectric actuators for maximum energy harvesting", *Smart Nano-Micro Mater. Dev.*, **8204**, 2011. <https://doi.org/10.1117/12.905087>.
- Khazaei, M., Rezaei, A. and Rosendahl, L. (2022), "Piezoelectric resonator design and analysis from stochastic car vibration using an experimentally validated finite element with viscous-structural damping model", *Sustain. Energy Technol. Assessm.*, **52**, 102228. <https://doi.org/10.1016/j.seta.2022.102228>.
- Lerch, R. (1988), "Finite element analysis of piezoelectric transducers", *EEE 1988 Ultrasonics Symposium Proceedings*, 643-654. <https://doi.org/10.1109/ULTSYM.1988.49457>.
- Lerch, R. (1990), "Simulation of piezoelectric devices by two- and three-dimensional finite elements", *IEEE Trans. Ultrason., Ferroel. Freq. Control*, **37**(3), 233-247. <https://doi.org/10.1109/58.55314>.
- Lin, Y.C., Tseng, K.S. and Ma, C.C. (2021), "Investigation of resonant and energy harvesting characteristics of piezoelectric fiber composite bimorphs", *Mater. Des.*, **197**, 109267. <https://doi.org/10.1016/j.matdes.2020.109267>.
- Luschi, L. and Pieri, F. (2014), "An analytical model for the determination of resonance frequencies of perforated beams", *J. Micromech. Microeng.*, **24**(5), 055004. <https://doi.org/10.1088/0960-1317/24/5/055004>.
- Machu, Z., Rubes, O., Sevecek, O. and Hadas, Z. (2021) "Experimentally verified analytical models of piezoelectric cantilevers in different design configurations", *Sensor.*, **21**(20), 6759. <https://doi.org/10.3390/s21206759>.
- Malekzadeh Fard, K., Khajehdehi Kavanroodi, M., Malek-Mohammadi, H. and Pourmoayed, A. (2022), "Buckling and vibration analysis of a double-layer graphene sheet coupled with a piezoelectric nanoplate", *J. Appl. Comput. Mech.*, **8**(1), 129-143. <https://doi.org/10.22055/JACM.2020.32145.1976>.
- Malikan, M. (2017), "Electromechanical shear buckling of piezoelectric nanoplate using modified couple stress theory based on simplified first order shear deformation theory", *Appl. Math. Model.*, **48**, 196-207.

- <http://doi.org/10.1016/j.apm.2017.03.065>.
- Malikan, M. and Eremeyev, V.A. (2020), "On Nonlinear bending study of a piezo-flexomagnetic nanobeam based on an analytical-numerical solution", *Nanomater.*, **10**(9), 1762. <https://doi.org/10.3390/nano10091762>
- Malikan, M. and Eremeyev, V.A. (2021), "Flexomagnetic response of buckled piezomagnetic composite nanoplates", *Compos. Struct.*, **267**, 113932. <https://doi.org/10.1016/j.compstruct.2021.113932>
- Mechkour, H. (2022), "Modeling of perforated piezoelectric plates", *Math. Comput. Appl.*, **27**(6), 100. <https://doi.org/10.3390/mca27060100>
- Meeker, T.R. (1996), "Publication and proposed revision of ANSI/IEEE standard 176-1987", *IEEE Trans. Ultrasonic. Ferroel. Freq. Control*, **43**(5), 717-772.
- Melaibari, A., Abdelrahman, A.A., Hamed, M.A., Abdalla, A.W. and Eltahir, M.A. (2022) "Dynamic analysis of a piezoelectrically layered perforated non-local strain gradient nanobeam with flexoelectricity", *Math.*, **10**(15), 2614. <https://doi.org/10.3390/math10152614>
- Mohammad, K.H. and Dehghani, R. (2022), "Distributed-parameter dynamic modeling and bifurcation analysis of a trapezoidal piezomagnetoelastic energy harvester", *J. Appl. Comput. Mech.*, **8**(1), 97-113. <https://doi.org/10.22055/JACM.2019.30823.1785>.
- Moory-Shirbani, M., Sedighi, H.M., Ouakad, H.M. and Najar, F. (2018), "Experimental and mathematical analysis of a piezoelectrically actuated multilayered imperfect microbeam subjected to applied electric potential", *Compos. Struct.*, **184**, 950-960. <https://doi.org/10.1016/j.compstruct.2017.10.062>.
- Nadeem, M., He, J.H., He, C.H., Sedighi, H.M. and Shirazi, A. (2022), "A numerical solution of nonlinear fractional newell-whitehead-segel equation using natural transform", *Twms J. Pure Appl. Math.*, **13**(2), 168-182.
- Najafi Ardekany, A. (2022), "Vibration stabilization of a flexible beam under fluid loading by utilizing piezoceramics", *Iran. J. Sci. Technol., Trans. Mech. Eng.*, **46**(4), 1001-1013. <https://doi.org/10.1007/s40997-021-00463-z>.
- Phung, M.V., Nguyen, D.T., Doan, L.T., Nguyen, D.V. and Duong, T.V. (2022), "Numerical investigation on static bending and free vibration responses of two-layer variable thickness plates with shear connectors", *Iran. J. Sci. Technol., Trans. Mech. Eng.*, **46**(4), 1047-1065. <https://doi.org/10.1007/s40997-021-00459-9>.
- Ramegowda, P.C., Ishihara, D., Takata, R., Niho, T. and Horie, T. (2020b), "Hierarchically decomposed finite element method for a triply coupled piezoelectric, structure, and fluid fields of a thin piezoelectric bimorph in fluid", *Comput. Meth. Appl. Mech. Eng.*, **365**, 113006. <https://doi.org/10.1016/j.cma.2020.113006>.
- Ramegowda, P.C., Ishihara, D., Takata, R. and Horie, T. (2021), "Hierarchical modeling and finite element analysis of piezoelectric energy harvester from structure-piezoelectric-circuit interaction", *14th WCCM-ECCOMAS Congress 2020*, January. <https://doi.org/10.23967/wccm-eccomas.2020.163>.
- Ramegowda, P.C., Ishihara, D., Takata, R., Niho, T. and Horie, T. (2020a), "Finite element analysis of a thin piezoelectric bimorph with a metal shim using solid direct-piezoelectric and shell inverse-piezoelectric coupling with pseudo direct-piezoelectric evaluation", *Compos. Struct.*, **245**, 112284. <https://doi.org/10.1016/j.compstruct.2020.112284>.
- Shabara, M., Rahman Badawi, A. and Xu, T.B. (2020), "Comprehensive piezoelectric material application issues on energy harvesting for artificial intelligence systems", *AIAA Scitech 2020 Forum*. <https://doi.org/10.2514/6.2020-1862>.
- Shevtsova, M., Nasedkin, A., Shevtsov, S., Zhilyaev, I. and Chang, S. (2016), "An optimal design of underwater piezoelectric transducers of new generation", *Proceedings of the 23rd International Congress on Sound and Vibration: From Ancient to Modern Acoustics*, Athens, Greece.
- Silva, P.B., Mencik, J.M. and Arruda, J.R. (2016), "On the use of the wave finite element method for passive vibration control of periodic structures", *Adv. Aircraft Spacecraft Sci.*, **3**(3), 299. <https://doi.org/10.12989/aas.2016.3.3.299>.
- Su, H., Sui, L., Song, P. and Lu, Y. (2019), "Theoretical analysis and experimental study of a perforated piezoelectric cantilever", *IOP Conf. Ser.: Mater. Sci. Eng.*, **563**(3), 032039.

899X/563/3/032039.

Wang, L., Wu, Z., Liu, S., Wang, Q., Sun, J., Zhang, Y., ... & Maeda, R. (2022), "Uniform stress distribution of bimorph by arc mechanical stopper for maximum piezoelectric vibration energy harvesting", *Energi.*, **15**(9), 3268. <https://doi.org/10.3390/en15093268>.

Wang, S.Y. (2004), "A finite element model for the static and dynamic analysis of a piezoelectric bimorph", *Int. J. Solid. Struct.*, **41**(15), 4075-4096. <https://doi.org/10.1016/j.ijsolstr.2004.02.058>.

CC

Abbreviations

MEMS	Micro Electromechanical Systems
PEH	Piezoelectric Energy Harvesting
FGM	Functionally Graded Material
PVEH	Piezoelectric Vibration Energy Harvester
PZT	Lead Zirconate Titanate
PVDF	Polyvinylidene Fluoride
IEEE	Institute of Electrical and Electronic Engineers
FEM	Finite Elements Method
ANSYS	Analysis of Systems a Software for Simulation

Symbols

L	Length
W	Width
h	Thickness
Y	Young's modulus
σ	Stress
ε	electric displacement, electric field, and dielectric permittivity of the material
E	Vector of applied electric field
d	piezoelectric matrix (charge density per applied stress)
S	Compliance matrix
D	Vector of electric displacement
K	Electromechanical Coupling Factor
A	Area
g	Piezoelectric Voltage Constant
α	Filling Ratio
N	The number of holes across the beam in the section
I	Moment of Inertia
ρ	Density
r	Mechanical Displacement Field
f_E	External Force
$\{\chi^e\}$	Mechanical degrees of freedom for each element

v_e	the electrode-to-electrode potential differential
$[m^e]$	Composition of the mass matrix of the elements
$[k_{qq}^e]$	Composition of the stiffness matrix of the elements
$[k_{q\phi}^e]$	Electromechanical coupling matrix element
$[c_a^e]$	Viscous damping matrix of the element
$[c_s^e]$	Matrix of structural damping elements
$K.E.$	Kinetic Energy
$P.E$	Potential Energy
W_{el}	Electrical Energy
W_E	External Mechanical Force